
Med-UniC: Unifying Cross-Lingual Medical Vision-Language Pre-Training by Diminishing Bias

Zhongwei Wan^{1*}, Che Liu^{2*}, Mi Zhang¹, Jie Fu⁵, Benyou Wang⁴, Sib0 Cheng²,
Lei Ma³, César Quilodrán-Casas², Rossella Arcucci²

¹The Ohio State University ²Imperial College London

³Peking University ⁴The Chinese University of Hong Kong, Shenzhen

⁵Beijing Academy of Artificial Intelligence

{wan.512, mizhang.1}@osu.edu, lei.ma@pku.edu.cn, wangbenyou@cuhk.edu.cn
{che.liu21, sib0.cheng, c.quilodran, r.arcucci}@imperial.ac.uk, fujie@baai.ac.cn

Abstract

The scarcity of data presents a critical obstacle to the efficacy of medical vision-language pre-training (VLP). A potential solution lies in the combination of datasets from various language communities. Nevertheless, the main challenge stems from the complexity of integrating diverse syntax and semantics, language-specific medical terminology, and culture-specific implicit knowledge. Therefore, one crucial aspect to consider is the presence of community bias caused by different languages. This paper presents a novel framework named Unifying Cross-Lingual Medical Vision-Language Pre-Training (**Med-UniC**), designed to integrate multi-modal medical data from the two most prevalent languages, English and Spanish. Specifically, we propose Cross-lingual Text Alignment Regularization (**CTR**) to explicitly unify cross-lingual semantic representations of medical reports originating from diverse language communities. **CTR** is optimized through latent language disentanglement, rendering our optimization objective to not depend on negative samples, thereby significantly mitigating the bias from determining positive-negative sample pairs within analogous medical reports. Furthermore, it ensures that the cross-lingual representation is not biased toward any specific language community. **Med-UniC** reaches superior performance across 5 medical image tasks and 10 datasets encompassing over 30 diseases, offering a versatile framework for unifying multi-modal medical data within diverse linguistic communities. The experimental outcomes highlight the presence of community bias in cross-lingual VLP. Reducing this bias enhances the performance not only in vision-language tasks but also in uni-modal visual tasks.

1 Introduction

English, despite not being the primary native language for a vast majority of the global population, remains the dominant language in vision-language pre-training (VLP) datasets. Uni-lingual VLP models not only demonstrate restricted performance in cross-lingual tasks, but also bring the community bias on non-English speaking populations (displayed in Fig 1), particularly in the context of medical applications.

Researchers have used machine-translated non-English corpora and techniques like masked language model (MLM) and contrastive learning to unify cross-lingual representations [1, 2, 3, 4]. However, MLM-based representations still separate languages, as shown in Fig 1a and

* Equal Contribution.

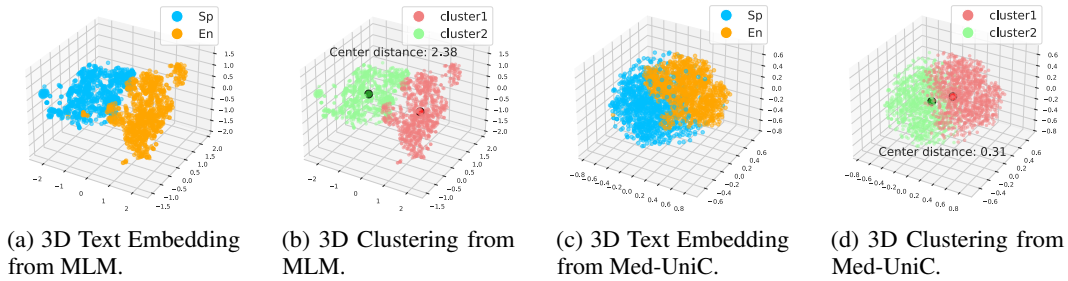


Figure 1: Graphical illustration of community bias in MLM and Med-UniC is shown with blue points representing Spanish reports and orange points indicating English reports, visualized via T-SNE. MLM denotes cross-lingual masked language modeling.

1b. Additionally, as highlighted in Fig 2, the significant similarity among reports from diverse communities suggests that the strict reliance on negative samples in contrastive learning could introduce more bias during text alignment. Hence, Med-UniC focuses on learning text invariants in VLP using negative-free text alignment to avoid the bias mentioned above. In this work, we introduce a unified framework named **Med-UniC**², designed to acquire language-agnostic representations from chest x-ray (CXR) scans and associated radiology reports. Med-UniC learns the representation from 3 perspectives: visual invariants, visual-textual invariants, and text invariants. Considering medical vision-language tasks, such as zero-shot image classification, are dependent on semantic information and language-independent, we propose **CTR** (Cross-lingual Text Alignment Regularization) to explicitly minimize linguistic disparities in cross-lingual representations within the latent space, as visualized in Fig 1c and 1d. Consequently, Med-UniC tackles non-English vision-language tasks without the model bias stemming from the language model (LM) pre-trained on predominantly English corpora. Additionally, we found that the unified cross-lingual representation enhances performance across a range of uni-modal visual tasks. This paper makes the following contributions:

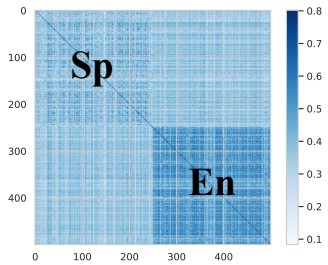


Figure 2: Similarity matrix for medical reports embedding from MLM.

- To the best of our knowledge, we are the first to empirically identify the existence of community bias originating from diverse languages in cross-lingual medical VLP (displayed in Fig 1), and the negative impact of community bias on both uni-modal and vision-language downstream tasks.
- We introduce the framework Med-UniC with CTR, designed to diminish community bias in medical VLP by unifying cross-lingual latent representations. Med-UniC achieves SOTA results in medical vision-language tasks across different languages, demonstrating its efficacy and broad applicability across various language communities.
- Med-UniC achieves SOTA results on all uni-modal visual tasks. This highlights the advantages of mitigating community bias and unifying cross-lingual representations in medical VLP, enabling robust and comprehensive learning of visual representations.
- Med-UniC effectively mitigates community bias without the requirement for manual curation or language-specific annotations. Importantly, Med-UniC enhances the accessibility of medical VLP to non-English speaking populations, circumventing potential biases that may arise from predominantly English datasets in traditional VLP.

2 Related Work

Medical VLP Complex medical reports and a shortage of large-scale medical image-text datasets have limited medical VLP research. Previous works such as ConVIRT [5] and GLoRIA [6] utilized

²The code will be released soon.

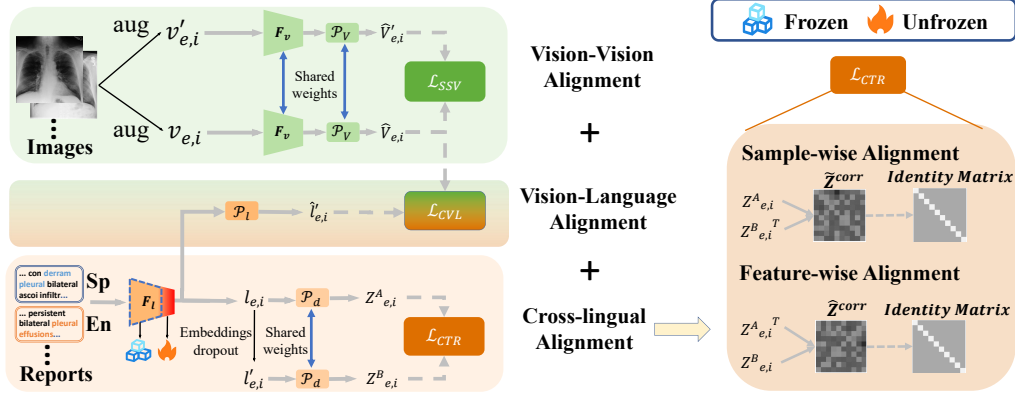


Figure 3: Overview Med-UniC. CVL, SSV, CTR represent *cross-lingual vision-language alignment*, *self-supervised vision alignment*, *Cross-lingual Text Alignment Regularization*, respectively.

contrastive objectives and global-local VLP to align image-text pairs. MGCA [7] used disease-level annotations for alignment, while MedKLIIP [8] manually extracted medically relevant entities. MRM [9] replaced alignment with a reconstruction task involving masked visual and textual tokens. However, these methods fail to capitalize on valuable cross-lingual knowledge and do not effectively unify cross-lingual representations. As a result, their performance on cross-lingual tasks is considerably limited.

Cross-lingual VLP Most recent cross-lingual VLP research has focused on a limited set of languages, with a few comparing natural cross-lingual VLP to English-only VLP [10]. Studies such as [1, 2, 3, 4] used machine-translated corpora and contrastive learning to generate language-agnostic representations. Yet, cross-lingual VLP in the medical domain remains unexplored mainly due to two main challenges: the limitations of machine translation for medical reports and the bias introduced by hard positive-negative pairs in contrastive learning. We propose CTR, a negative-free disentangled loss method, to unify cross-lingual text representations, addressing these issues.

Large General Model Recently, there have been impressive advances in large general models for language and vision tasks, such as ChatGPT [11], SAM, and DINOv2 [11, 12, 13]. However, these models still face significant limitations in the medical domain due to their lack of domain-specific knowledge and inability to jointly process visual and textual information [14, 15, 16]. ChatGPT [11] and SAM [12], currently limited to single-modality input, are unsuitable for vision-language tasks. While SAM excelled at instance segmentation, it struggled with medical image pathology segmentation [17, 18, 16]. Conversely, Med-UniC addressed these constraints by utilizing visual and textual data, integrating domain-specific knowledge without the high computational expenses of large general models. Surprisingly, Med-UniC outperformed the extensive vision model, DINOv2 [13], trained on 1.2B images with 1B parameters, by a considerable margin in multiple visual tasks. This suggests that Med-UniC is a more effective and efficient solution compared to large general models.

3 Method

3.1 Overall Framework of Med-UniC

Our Med-UniC framework aims to learn cross-lingual medical representation from CXR images and paired radiology reports. Given a training set of N cross-lingual dataset $S \in \mathcal{V} \times \mathcal{L}$ consisting of pairs $(v_{e,i}, l_{e,i})$, where \mathcal{V} and \mathcal{L} are visual and text set, respectively, $v_{e,i}$ is a raw image and $l_{e,i}$ is a text report, e belongs to language domain (e.g., Spanish or English), $i \in N$. The Med-UniC architecture mainly consists of an image encoder $\mathcal{F}_v: \mathcal{V} \mapsto \mathbb{R}^{D_v}$ to encode the raw image into the embeddings with dimension D_v , and a cross-lingual text encoder $\mathcal{F}_l: \mathcal{L} \mapsto \mathbb{R}^{D_l}$ to encode the text report to the embeddings with dimension D_l . Then $S = \{(\mathbf{v}_{e,1}, \mathbf{l}_{e,1}), (\mathbf{v}_{e,2}, \mathbf{l}_{e,2}), \dots, (\mathbf{v}_{e,N}, \mathbf{l}_{e,N})\}$, where $\mathbf{v}_{e,i} = \mathcal{F}_v(v_{e,i})$ and $\mathbf{l}_{e,i} = \mathcal{F}_l(l_{e,i})$.

As depicted in Fig 3, Med-UniC incorporates three concurrent alignment strategies: *cross-lingual vision-language alignment*, *self-supervised vision alignment*, and *cross-lingual text alignment regularization*. For cross-lingual vision-language alignment, we extend the text encoder from uni-lingual into a cross-lingual style, which can equip the model with cross-lingual cross-modal ability by pulling

the embeddings of paired image-reports pairs together while pushing apart embeddings of unmatched pairs, under the loss \mathcal{L}_{CVL} . Meanwhile, we employ self-supervised vision alignment, leveraging the loss \mathcal{L}_{SSV} , to enhance the robustness of visual representation [19]. More importantly, we introduce a cross-lingual text alignment regularization, encompassing sample-level and feature-level approaches, to mitigate community bias stemming from different languages. This regularization is supervised by the loss \mathcal{L}_{CTR} . The learning objective of Med-UniC integrates the three strategies mentioned above and can be formulated as follows:

$$\mathcal{L} = \mathcal{L}_{CVL} + \mathcal{L}_{SSV} + \mathcal{L}_{CTR} \quad (1)$$

This training scheme compels Med-UniC to assimilate information from diverse perspectives, fostering a robust cross-modal, cross-lingual framework that concurrently learns visual invariants, visual-textual invariants, and text invariants.

3.2 Cross-lingual Vision-language Alignment

Cross-lingual Medical LM To initialize Med-UniC with the ability to process different languages and learn fundamental cross-lingual syntactic and semantic knowledge. We select CXR-BERT [20], a uni-lingual LM pre-trained on a large-scale biomedical corpus, as our text encoder and further adapted it for cross-lingual operation. The concrete steps proceed as follows: **(1)** Constructing a cross-lingual vocabulary set \mathcal{T} : we collected the radiology reports of the second language (e.g., Spanish PadChest dataset [21]), which is seldom used for medical pre-training compared to English dataset [22, 23]. Then we leverage a general Spanish Spacy³ to build a tokenizer and make use of TF-IDF tool⁴ to generate M ranked new tokens $\mathcal{T}_{sp} = \{t_{sp}^1, t_{sp}^2, \dots, t_{sp}^M\}$ according to their importance from multiple reports. **(2)** Building new wording embeddings \mathbf{W} : we augment the original vocabulary \mathcal{T}_{en} with the sorted Spanish tokens to generate $\mathcal{T} = \{\mathcal{T}_{en}, \mathcal{T}_{sp}\}$ then expand a length of M random initialized vectors \mathbf{W}_{sp} on CXR-BERT’s word embeddings \mathbf{W}_{en} , where $\mathbf{W} = [\mathbf{W}_{en}; \mathbf{W}_{sp}]$. **(3)** Masked Cross-lingual Modeling: we following BERT [24], randomly mixed English [22] and Spanish [21] medical reports as pre-train corpus. Then we randomly choose tokens in the mixed sequences, replace them with the [MASK] token and set 15% masking probability as in BERT [25]. We selectively update several high layers to alleviate catastrophic forgetting [26] during vision-language pre-training. More details will be show in Sec 4.5.

Vision-Language Alignment Following CLIP framework [27], we incorporate a contrastive learning object to predict the matched pair $(v_{e,i}, l_{e,i})$ from $N \times N$ possible image-text pairs while mapping $N^2 - N$ negative pairs far apart. Specifically, two non-linear visual and linguistic projectors \mathcal{P}_l and \mathcal{P}_v are used to transform $\mathbf{v}_{e,i}$ and $\mathbf{l}_{e,i}$ into the same dimension d , where $\hat{\mathbf{v}}_{e,i} = \mathcal{P}_v(\mathbf{v}_{e,i})$, $\hat{\mathbf{l}}_{e,i} = \mathcal{P}_l(\mathbf{l}_{e,i})$, and $\hat{\mathbf{v}}_{e,i}, \hat{\mathbf{l}}_{e,i} \in \mathbb{R}^d$. Obtaining image feature vectors $[\hat{\mathbf{v}}_{e,i}]_{i=1}^N$ and text feature vectors $[\hat{\mathbf{l}}_{e,i}]_{i=1}^N$ from a training batch, we compute cosine similarities $s_{i,i}^{v2l} = \hat{\mathbf{v}}_{e,i}^\top \hat{\mathbf{l}}_{e,i}$ and $s_{i,i}^{l2v} = \hat{\mathbf{l}}_{e,i}^\top \hat{\mathbf{v}}_{e,i}$, representing image-text and text-image similarities, respectively. \mathcal{L}_{CVL} is then formulated as follows:

$$\mathcal{L}_v^{v2l} = -\log \frac{\exp(s_{i,i}^{v2l}/\sigma_1)}{\sum_{j=1}^K \exp(s_{i,j}^{v2l}/\sigma_1)}, \mathcal{L}_i^{l2v} = -\log \frac{\exp(s_{i,i}^{l2v}/\sigma_1)}{\sum_{j=1}^K \exp(s_{i,j}^{l2v}/\sigma_1)} \quad (2)$$

$$\mathcal{L}_{CVL} = \frac{1}{2K} \sum_{i=1}^K (\mathcal{L}_v^{v2l} + \mathcal{L}_i^{l2v}), \quad (3)$$

where \mathcal{L}_v^{v2l} and \mathcal{L}_i^{l2v} are image-text and text-image InforNCE [28] contrastive loss, respectively. σ_1 is the temperature hyper-parameter set to 0.07 in our experiments, K is the batch size for each step and $K \in N$. Through overall loss \mathcal{L}_{CVL} , the model learns maximal mutual information between the matched image-text pairs containing cross-lingual attributes within a batch.

3.3 Self-supervised Vision Alignment

To obtain more exhaustive visual representation, we include visual invariant learning as a parallel objective during VLP. Drawing inspiration from [19], we initially apply random augmentations (such as random cropping and flipping) to the original images to create augmented views as positive pairs $[(v_{e,i}, v'_{e,i})]_{i=1}^N$, while treating the rest of the images in the mini-batch as negative samples. We

³<https://spacy.io/models/es-dep-news-trf>

⁴TfidfVectorizer: <https://scikit-learn.org/>

follow the data augmentation strategy as per [19]. Subsequently, we extract the representations of the augmented views $[\hat{\mathbf{v}}']_{i=1}^N$ using the vision projector p_v and vision encoder \mathcal{F}_v , similar to $[\hat{\mathbf{v}}]_{i=1}^N$. Therefore, the visual invariant learning objective becomes:

$$\mathcal{L}_{SSV} = -\frac{1}{K} \sum_{j=1}^N \log \frac{\exp(s_{i,i}^{v2v'} / \sigma_2)}{\sum_{j=1}^N \exp(s_{i,j}^{v2v'} / \sigma_2)}, s_{i,i}^{v2v'} = \hat{\mathbf{v}}_{e,i}^\top \hat{\mathbf{v}}'_{e,i} \quad (4)$$

where σ_2 is the temperature hyper-parameter also set to 0.07 for overall loss objective \mathcal{L}_{SSV} .

3.4 Cross-lingual Text Alignment Regularization

As illustrated in Fig 1, and corroborated by research in natural language processing [29, 30], cross-lingual text representations tend to form distinct clusters based on their respective languages. This trend introduces a community bias within data from different language communities, even when no explicit language attribute is provided. This suggests that VLP processes medical data based on their language community, risking unfairness in clinical applications and potentially decreasing downstream task performance in both uni-modal and vision-language tasks [31, 32, 33]. To mitigate this bias and potential risks, we introduce *Cross-lingual Text Alignment Regularization* (CTR) to learn language-independent text representations and neutralize the adverse effects of community bias on other modalities. CTR comprises three components:

Text augmentation We first adopt the dropout strategy [34] to generate augmented the text representation $\mathbf{l}'_{e,i}$ from the text encoder and obtain the matched pairs $[(\mathbf{l}_{e,i}, \mathbf{l}'_{e,i})]_{i=1}^N$, and then a separate linguistic projector \mathcal{P}_d designed for de-correlation is leveraged to generate two different view pairs $[(\mathbf{Z}_{e,i}^A, \mathbf{Z}_{e,i}^B)]_{i=1}^N$, where $\mathbf{Z}_{e,i}^A = \mathcal{P}_d(\mathbf{l}_{e,i})$, $\mathbf{Z}_{e,i}^B = \mathcal{P}_d(\mathbf{l}'_{e,i})$, and the new feature dimension $D' > D$.

Text-feature alignment To further alleviate information redundancy [35, 36] and obtain the shared cross-lingual text representation, we first normalize the augmented embedding pairs $\{\mathbf{Z}_e^A, \mathbf{Z}_e^B\} \in \mathbb{R}^{N \times D'}$ along the batch K dimension so that each feature dimension has a zero-mean and $1/\sqrt{K}$ standard deviation distribution to generate $\tilde{\mathbf{Z}}_e$, and then compute their cross-correlation $\tilde{\mathbf{Z}}_e^{corr} = \tilde{\mathbf{Z}}_e^{AT} \tilde{\mathbf{Z}}_e^B$. The formulas of feature-dimension decorrelation can be defined as:

$$\mathcal{L}_{TF} = \frac{1}{D'} \left\{ \underbrace{\sum_j^{D'} \left(1 - \sum_i^K \tilde{\mathbf{Z}}_{e,i}^{A,jT} \tilde{\mathbf{Z}}_{e,i}^{B,j} \right)^2}_{\text{cross-lingual invariance}} + \lambda \underbrace{\sum_j^{D'} \sum_{i \neq j}^K \tilde{\mathbf{Z}}_{e,i}^{A,jT} \tilde{\mathbf{Z}}_{e,i}^{B,j}}_{\text{cross-lingual gap reduction}} \right\}, \quad \tilde{\mathbf{z}}_e = \frac{\mathbf{Z}_e - \mu_K(\mathbf{Z}_e)}{\sqrt{K} \sigma(\mathbf{Z}_e)} \quad (5)$$

The first term's objective is to learn a language-invariant representation by optimizing the diagonal elements of the correlation matrix to equal one. Simultaneously, the second term aims to shrink the cross-lingual gap and optimize information utilization in each latent dimension by driving the off-diagonal elements towards zero. Finally, We normalize the loss along with the feature dimension D' .

Text-to-text alignment: Similarly, the text-to-text alignment decorrelates the cross-correlation matrix along with feature dimension D' , and $\hat{\mathbf{Z}}_e$ is the normalized embeddings, $\hat{\mathbf{Z}}_e^{corr} = \hat{\mathbf{Z}}_e^A \hat{\mathbf{Z}}_e^{BT}$:

$$\mathcal{L}_{TT} = \frac{1}{K} \left\{ \underbrace{\sum_j^K \left(1 - \sum_i^{D'} \hat{\mathbf{Z}}_{e,i}^{A,j} \hat{\mathbf{Z}}_{e,i}^{B,jT} \right)^2}_{\text{text instance alignment}} + \lambda \underbrace{\sum_j^K \sum_{i \neq j}^{D'} \hat{\mathbf{Z}}_{e,i}^{A,j} \hat{\mathbf{Z}}_{e,i}^{B,jT}}_{\text{text consistency regularizer}} \right\}, \quad \hat{\mathbf{z}}_e = \frac{\mathbf{Z}_e - \mu_{D'}(\mathbf{Z}_e)}{\sqrt{D'} \sigma(\mathbf{Z}_e)} \quad (6)$$

where the *text instance alignment* term attempts to maximize the mutual information of a batch of cross-lingual text samples, and the *text consistency regularizer* can also be deemed as the text in-modal consistency [37] by reducing the mismatched text pairs into 0 in a batch K . Where λ in Eq 5, 6, is a non-negative hyperparameter trading off two terms. We also normalize the loss with the

batch dimension K . Therefore, the loss of *Cross-lingual Text Alignment Regularization* \mathcal{L}_{CTR} is:

$$\mathcal{L}_{CTR} = \mathcal{L}_{TF} + \mathcal{L}_{TT} \tag{7}$$

4 Experiments

4.1 Pre-training Configuration

Dataset We pre-train Med-UniC framework using MIMIC-CXR [38], which contains CXR images and their corresponding radiology reports in English. Also, we involve PadChest [39], which includes CXR images and their corresponding radiology reports in Spanish. Both datasets are pre-processed following the approach described in [5, 6, 7], including image resizing, pixel value normalization, and text tokenization. Additionally, the dataset is filtered by excluding lateral views and reports with less than three tokens. This results in a pre-training dataset of approximately 220k image-text pairs for MIMIC-CXR [38] and 160k pairs for PadChest [39].

Implementation In the VLP stage, we employ ResNet-50 [40] and ViT [41] as the vision backbones. We report the linear classification results for these two vision encoders to illustrate the model-agnostic capabilities of Med-UniC. Med-UniC is trained over 50 epochs using an early stop strategy on 16 V100 GPUs with a batch size of 128 per GPU. We utilize AdamW [42] as the optimizer, setting the learning rate to $4e^{-5}$ and the weight decay to $5e^{-2}$. A linear warm-up and cosine annealing scheduler are also deployed in this process. Additionally, The coefficients λ is set to $5.1e^{-3}$ following [36].

4.2 Downstream Tasks

Medical Image Linear Classification We perform this task on CheXpert [23], RSNA [43], and COVIDx [44] datasets. Following the previous work [6, 5, 7], we only update the parameter of a random initialized linear layer for classification and freeze the pre-trained vision backbone. We report the AUC scores (AUC) on CheXpert and RSNA and accuracy (ACC) on COVIDx as the evaluation metric following [6, 7].

Medical Image Zero-shot Classification We conduct this experiment on the CXP500 [45] and PDC [39] datasets, which comprise CXR images annotated by clinicians from English-speaking and Spanish-speaking countries, respectively. To circumvent prompt bias, we designate English positive prompt as ‘{disease}’ and negative prompt as ‘No {disease}’. Prompts in Spanish are prepared by native Spanish speakers, with the disease indicated as ‘{disease}’ and the negative prompt represented as ‘No hay {disease}’. Med-UniC is evaluated using both English and Spanish prompts across the two datasets, with additional experimental details provided in the Appendix. The results are represented as the macro average of AUC and F1 scores across all categories.

Medical Image Semantic Segmentation This task is performed on the RSNA [43] and the SIIM [46] datasets, following the data preprocessing in [7, 6]. Identical to [6, 7], the U-Net [47] fine-tuning settings are adopted for segmentation. All pre-trained vision backbones are considered as frozen encoders, and only the decoders of U-Net are updated during the fine-tuning. The segmentation performance is evaluated using Dice scores (Dice).

Medical Image Object Detection This task is performed on the RSNA [43] and Object-CXR [48] datasets, following the same preprocessing of [7]. Same as [7], we utilize YOLOv3 [49] as the detection architecture, using our pre-trained vision encoder as the backbone and only updating the detection head during fine-tuning. Mean Average Precision (mAP) with IOU thresholds 0.4~0.75, is adopted to evaluate the detection task.

For all downstream tasks, except zero-shot classification, we fine-tune with 1%, 10%, 100% of the training data. More downstream tasks’ settings, including split information and train/valid/test set details, can be found in the Appendix.

4.3 Comparison to the state-of-the-art

Zero-shot Classification To assess the cross-lingual visual-textual representation learned from Med-UniC, we implement the zero-shot image classification task on two CXR datasets, which originate from distinct linguistic communities and utilize different language prompts. Tab 1 illustrates that Med-UniC surpasses all SOTA methods on both datasets, regardless of the language setting or the

Table 1: Zero-shot Image Classification results. F1 and AUC scores are reported. Best results of each setting are in boldface. ‘En’ and ‘Sp’ respectively stand for prompts in English and Spanish languages. Methods with * leverage disease-level annotations for pre-training.

Method	CXP500(En)		CXP500(Sp)		PDC(En)		PDC(Sp)	
	AUC	F1	AUC	F1	AUC	F1	AUC	F1
ConVIRT[5]	59.5	19.2	60.5	15.8	45.1	26.5	49.1	12.6
GLoRIA[6]	43.2	2.4	40.2	16.1	52.3	10.1	50.3	8.2
GLoRIA-MIMIC [6]	46.2	5.5	51.5	20.3	53.1	12.1	52.2	11.3
MGCA* [7]	72.1	6.5	50.4	22.3	46.4	32.5	49.8	26.1
MedKILP* [8]	70.5	14.7	55.6	21.9	50.5	28.7	51.7	25.8
MRM [9]	65.2	10.4	48.3	16.1	50.1	24.6	51.4	25.1
Ours	75.4	30.3	71.3	32.2	72.9	42.6	71.4	37.1

linguistic community data source. Across both datasets, Med-UniC delivers an average increase of over 20% in the F1 score when using English prompts and more than 15% when using Spanish prompts. This showcases the effectiveness and adaptability of Med-UniC in managing cross-lingual vision-language tasks.

Interestingly, the AUC score of other SOTA methods experiences a substantial drop when the prompts transition from English to Spanish on CXP500 [45], a dataset collected from English-speaking communities. Similarly, all compared methods show comparably poor performance on PDC [39], a dataset derived from Spanish-speaking communities. MedKLIP [8], despite its commendable performance on the CXP500 [45] in the English setting due to its supervised pre-training with disease annotation, persistently shows a drop in performance on both the CXP500 [45] and PDC [39] when Spanish prompts are used, and also on the PDC [39] when using English prompts. These results highlight the significant community bias inherent in uni-lingual medical VLP models, even those utilizing annotations for pre-training. This bias adversely impacts the diagnostic quality when dealing with patients from non-English-speaking communities or those who do not speak English.

The unsatisfied performance of the compared methods also suggests that these models might incorporate linguistic community attributes during VLP, which negatively influences the learning of semantic meanings. Consequently, As a result, these models have difficulties in effectively interpreting CXR scans or prompts from non-English communities, which substantially limits the models’ transferability. Further analysis can be found in Sec 4.4.

Table 2: Linear classification results for CheXpert, RSNA, and COVIDx datasets with 1%, 10%, and 100% training data. The best results are highlighted in bold. A standard ResNet-50 backbone is denoted as *CNN-based*. Methods with * leverage disease-level annotations for pre-training.

Method	CheXpert (AUC)			RSNA (AUC)			COVIDx (ACC)		
	1%	10%	100%	1%	10%	100%	1%	10%	100%
Random Init	56.1	62.6	65.7	58.9	69.4	74.1	50.5	60.3	70.0
ImageNet Init	74.4	79.7	81.4	74.9	74.5	76.3	64.8	78.8	86.3
<i>CNN-based</i>									
GLoRIA [6]	86.6	87.8	88.1	86.1	88.0	88.6	67.3	77.8	89.0
ConVIRT [5]	85.9	86.8	87.3	77.4	80.1	81.3	72.5	82.5	92.0
GLoRIA-MIMIC [6]	87.1	88.7	88.0	87.0	89.4	90.2	66.5	80.5	88.8
MedKLIP* [8]	86.2	86.5	87.7	87.3	88.0	89.3	74.5	85.2	90.3
MGCA* [7]	87.6	88.0	88.2	88.6	89.1	89.9	72.0	83.5	90.5
Med-UniC (ResNet-50)	88.2	89.2	89.5	89.1	90.4	90.8	76.5	89.0	92.8
<i>ViT-based</i>									
MRM [9]	88.5	88.5	88.7	91.3	92.7	93.3	66.9	79.3	90.8
MGCA* (ViT-B/16) [7]	88.8	89.1	89.7	89.1	89.9	90.8	74.8	84.8	92.3
Med-UniC (ViT-B/16)	89.4	89.7	90.8	91.9	93.1	93.7	80.3	89.5	94.5
Med-UniC (ViT-L/32)	89.9	90.5	91.2	92.2	93.8	94.5	81.5	91.8	95.2

Medical Image Linear Classification To assess the quality of the visual representations learned by Med-UniC, we employ linear classification [50] on CheXpert [23], RSNA [43], and COVIDx [44]. As illustrated in Tab 2, Med-UniC framework consistently surpasses all uni-lingual pre-trained baselines across various settings and vision backbones. Significantly, even when MedKLIP [8] employs supervised VLP with disease-level annotation, Med-UniC consistently surpasses MedKLIP [8] across

Table 3: Results of semantic segmentation on SIIM and RSNA datasets and object detection on RSNA and Object-CXR datasets. The best results for each setting are highlighted in bold, and the '-' denotes mAP values smaller than 1%. Methods with * leverage disease-level annotations.

Method	Semantic Segmentation (Dice)						Object Detection (mAP)					
	SIIM			RSNA			RSNA			Object CXR		
	1%	10%	100%	1%	10%	100%	1%	10%	100%	1%	10%	100%
Random	9.0	28.6	54.3	6.9	10.6	18.5	1.0	4.0	8.9	-	0.5	4.4
ImageNet	10.2	35.5	63.5	34.8	39.9	64.0	3.6	8.0	15.7	-	2.9	8.3
ConVIRT[5]	25.0	43.2	59.9	55.0	67.4	67.5	8.2	15.6	17.9	-	8.6	15.9
GLoRA[6]	35.8	46.9	63.4	59.3	67.5	67.8	9.8	14.8	18.8	-	10.6	15.6
GLoRIA-MIMIC [6]	37.4	57.1	64.0	60.3	68.7	68.3	11.6	16.1	24.8	-	8.90	16.6
MGCA* [7]	49.7	59.3	64.2	63.0	68.3	69.8	12.9	16.8	24.9	-	12.1	19.2
MedKLIP* [8]	50.2	60.8	63.9	66.2	69.4	71.9	8.9	16.3	24.5	-	7.1	11.6
Ours	56.7	62.2	64.4	72.6	74.4	76.7	16.6	22.3	31.1	6.6	13.3	21.6

Table 4: Ablation study of Med-UniC on linear classification, semantic segmentation and zero-shot classification. The best results of each setting are in boldface.

SSV	Learning Objective			COVIDx (ACC)			RSNA (AUC)			SIIM (Dice)			CXP500 (F1)		PDC (F1)	
	CVL	CTR	MLM	1%	10%	100%	1%	10%	100%	1%	10%	100%	Sp	En	Sp	En
	✓		✓	72.8	85.5	91.8	87.7	88.5	89.4	51.9	56.5	58.7	63.5	59.8	62.2	58.5
✓	✓		✓	74.5	85.8	92.2	88.1	89.3	89.9	53.4	58.7	60.1	68.5	62.1	64.6	61.7
✓	✓	✓		75.0	84.3	92.5	88.2	89.6	89.7	53.8	59.6	61.5	70.3	65.9	65.4	63.7
✓	✓	✓	✓	76.5	89.0	92.8	89.1	90.4	90.8	56.7	62.2	64.4	75.4	71.3	72.9	71.4

all tasks and settings. This exemplifies the adaptability and efficacy of the visual representations cultivated by Med-UniC. Furthermore, this implies that unifying cross-lingual text representations via CTR can also improve the performance of uni-modal visual tasks.

Medical Image Semantic Segmentation and Object Detection In Tab 3, we further assessed the representation acquired by Med-UniC on segmentation and detection tasks. Impressively, Med-UniC outperforms all SOTA methods across every data fraction in all four tasks. Notably, Med-UniC achieves a Dice score of 72.6% on RSNA segmentation with only 1% data fine-tuning, exceeding the performance of all other SOTA methods fine-tuned on 100% data. Furthermore, Med-UniC reaches a 6.6% mAP on the Object-CXR dataset using just 1% data fine-tuning, surpassing other methods that barely achieve a 1% mAP. These findings further highlight the advantageous effects of unifying cross-lingual representations on vision-language tasks and uni-modal visual tasks.

4.4 Ablation Study and Bias Analysis

In this section, we ablate components of Med-UniC and present their performance on linear classification, zero-shot image classification, and semantic segmentation in Table 4. In all tasks, the combinations of all learning objectives achieve the highest performance, highlighting each component’s crucial role in Med-UniC. Med-UniC, when integrated with CTR, significantly outperforms the version with MLM in zero-shot tasks and nearly all uni-modal visual tasks.

To further investigate the influence of CTR and MLM, we randomly select 1000 English and 1000 Spanish image-text pairs. We then illustrate the text and image embeddings in Fig 1 and Fig 4, respectively. Surprisingly, when the text encoder is pre-trained with MLM, we notice that the medical report embeddings tend to cluster by their respective languages, as shown in Fig 1a,1b. However, when employing CTR, the embeddings from diverse language reports draw nearer, leading to a reduction in the distance between the two clusters compared to the embeddings produced by MLM, as shown in Fig 1c,1d. This clear pattern illustrates CTR’s ability to unify cross-lingual text representation within the latent space. Intriguingly, when pre-trained with CTR, the image embeddings become less distinguishable by their language community. In contrast, they form separate clusters according to their language community when pre-training does not involve

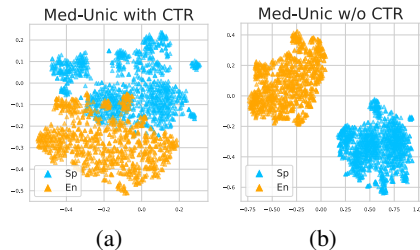


Figure 4: Visualization of image embeddings with or without CTR.

CTR. This observation implies that community bias affects not only the text modality but also the visual modality, as shown in Fig 4. Consequently, the reduction in community bias contributes to superior performance across all tasks when Med-UniC is pre-trained with all learning objectives. More details can be found in the Appendix.

4.5 Further Analysis

Visualization of Language-agnostic Visual-textual Attention We utilize Grad-CAM [51] to illustrate the areas in CXR images corresponding to various disease terminologies in both English and Spanish, as shown in Fig 5. Evidently, Med-UniC can accurately capture relevant regions that align closely with the indicated disease, exhibiting robustness across various languages. Consequently, the consistent cross-lingual visual-textual representations cultivated by Med-UniC underscore its outstanding generalizability across multiple downstream tasks and language communities.

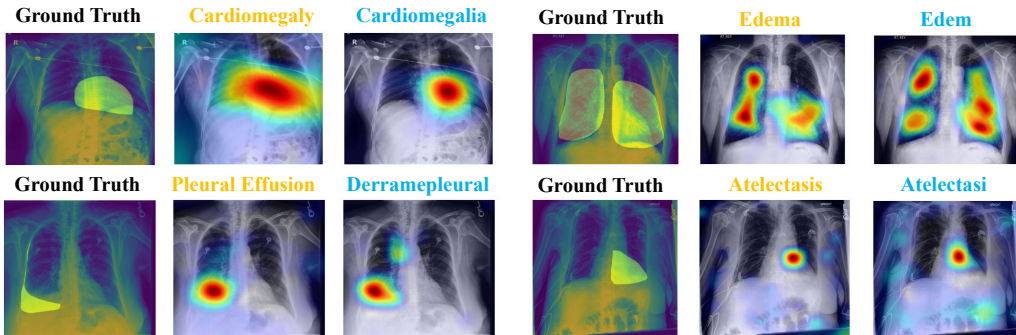


Figure 5: Attention heat-maps of the visual-textual association learned by Med-UniC, compared with ground truth annotations provided by clinicians. The blue and orange words denote Spanish and English types, respectively.

Table 5: Comparison with large vision model.

Method	CheXpert		RSNA		COVIDx	
	10%	100%	10%	100%	10%	100%
DINOv2 [52]	81.6	83.2	84.5	86.3	85.0	92.2
Med-UniC(ViT-B/16)	89.7	90.8	93.1	93.7	89.5	94.5
Med-UniC(ViT-L/32)	90.5	91.2	93.8	94.5	91.8	95.2

Table 6: Results of Med-UniC with different numbers of frozen layers.

Frozen layers	COVIDx (AUC)		RSNA (Dice)	
	10%	100%	10%	100%
0	87.7	92.5	75.0	75.8
6	88.0	92.3	74.3	76.3
9	89.0	92.8	74.4	76.7
12	87.1	90.5	72.3	74.4

Comparison with Large Vision Model In a comparison with DINOv2 [52], a large vision model trained on 1.2 billion images and comprising 1 billion parameters, Med-UniC outperforms it in linear classification tasks across all datasets, using different data ratios and two ViT backbones, as shown in Tab 5. This demonstrates the remarkable effectiveness of Med-UniC, even in scenarios with limited domain-specific data.

Impact of Frozen Layers for LM To investigate the impact of freezing layers in LM, we experimented with freezing various numbers (0, 6, 9, 12) in a 12-layer LM. Tab 6 shows that updating the last three layers offers better results comparable to updating more layers, hinting that updating more might cause catastrophic forgetting [26, 53] of cross-lingual MLM-acquired semantics. Performance declined when all layers were frozen, indicating the necessity of properly updating layers.

Error Bars We conducted three separate runs of Med-UniC, using different random seeds and ResNet-50 as the vision backbone for three tasks. We then reported the average metric and its standard deviation. As indicated in Tab 7, the variability between different task runs is relatively minor, demonstrating that Med-UniC consistently performs well in a variety of experiment configurations.

Table 7: Error bars analysis of linear classification, semantic segmentation, and object detection .

Ratio	COVIDx(ACC)	RSNA(Dice)	Object CXR(mAP)
1%	76.54±0.32	72.60±0.33	6.62±0.67
10%	89.01±0.16	74.43±0.19	13.34±0.27
100%	92.82±0.35	76.67±0.45	21.63±0.24

5 Conclusion

This work is the first to identify community bias in medical VLP stemming from diverse language communities and illustrates its negative impact on various downstream tasks. We present Med-UniC, a novel cross-lingual medical VLP framework, along with CTR, intended to unify cross-lingual text representations and mitigate language-driven community bias. This bias impacts both text and visual modalities, thereby affecting performance across vision-language and uni-modal visual tasks. The superior performance of Med-UniC across various tasks and data ratios underscores its efficiency and effectiveness. Through comprehensive ablation studies, we show that CTR significantly enhances performance in both vision-language and uni-modal visual tasks by effectively reducing community bias. This study provides a robust cross-lingual medical VLP framework and emphasizes the importance of inclusivity beyond English-speaking communities.

A Appendix Overview

In the supplementary material section, we first discuss the social impact and limitations of Med-UniC framework. Then, we introduce the details of the pre-training stage, including cross-lingual MLM pre-training and VLP for Med-UniC. Then we present the detailed configurations of several downstream tasks. Next, we conduct some additional experimental analysis.

B Discussion

Social impact Our Med-UniC framework presents an innovative solution for unifying CXR images and corresponding medical reports from diverse communities that use different languages, thereby addressing the data shortage in the medical VLP domain. Further investigations reveal that existing VLP models exhibit biased performance across various linguistic communities, even when pre-trained on cross-lingual data. However, Med-UniC effectively minimizes this bias, enhancing performance not only in cross-lingual tasks but also in uni-modal tasks. In essence, our work offers more than just a strategy for integrating data from different sources; it shines a light on the significant issue of community bias in cross-lingual VLP, calling for more fair and equitable practices in this field.

Limitation Our research primarily concentrates on cross-lingual medical VLP, limiting the number of languages, medical images, and reports included due to the current lack of public datasets. We’ve conducted comprehensive experiments involving uni-modal visual and vision-language tasks, but have not ventured into uni-modal language tasks like report generation. Looking ahead, we aim to expand our work to include more languages in the medical VLP and take on more challenging tasks, such as zero-shot guided segmentation or object detection. This area of our work, thus, acknowledges room for further development and exploration.

Future work Exploring these methods on diverse modality medical data such as electrocardiograms paired with clinical monitor records is an interesting future direction [54]. Furthermore, the alignment of different modality data can be viewed as a data fusion task, a commonly addressed issue in physics [55, 56, 57] or recommendation system [58].

C Implementation details for Pre-Training

C.1 Implementation for Cross-lingual MLM

Medical Report Pre-processing We prepare the cross-lingual pre-training corpus from the medical reports of MIMIC (En) [38] and PadChest (Sp) [39]. Specifically, we concatenate the findings and impression to form English medical reports for MIMIC. As for PadChest, we treat their radiology reports as Spanish reports. Examples of these reports can be seen in Fig 6 and Fig 7. To create the MLM corpus, we combine all the reports and shuffle them at the report-level.

MLM Pre-training Setup To obtain cross-lingual medical LM, we train the cross-linguistic encoder with the combined corpus using an Adam optimizer and adopt a linear warm-up scheduler. Specifically, the learning rate is $5e-4$, and the learning rate linearly increases from 0 to the peak value with a linear warm-up. Additionally, the max length for input tokens is 256. The MLM process is conducted

on 8 V100 GPUs and pre-trained within 15 epochs. To save GPU memory and speed up training, we adopt automatic mixed-precision FP16. The details of cross-lingual MLM are shown in Tab 8.

Table 8: Hyper-parameters of Cross-lingual MLM

Hyperparameters	
Training epochs	15
Total Batch size	1024
Number of GPUs	8
Gradient Accumulation	16
Maximum Sequence Length	256
Learning Rate	5e-4
Learning Rate Optimizer	Adam
Schedule	Linear Warm-up
Warm-up Proportion	10%
Adam Epsilon	1e-8
Masked Rate	0.15
FP16	True

Table 9: Hyper-parameters of VLP

Hyperparameters	
Pre-training epochs	50
Batch size per GPU	128
Number of GPUs	16
Gradient Accumulation	2
Maximum Sequence Length	256
Learning Rate	4e-5
Learning Rate Optimizer	AdamW
schedule	CosineAnnealing
Weight Decay	5e-2
FP16	True
Frozen Linguistic Encoder Layers	9
λ	5.1e-3
VL Alignment Dimension	512
CTR Embedding Dimension	1024

C.2 Implementation for Vision-language Pre-training

Model Architecture Following the same framework as CLIP [27], we utilize ResNet-50 [40], ViT-B/16 and ViT-L/32 [41] as our visual encoder, and we further pre-train CXR-BERT [20] via cross-lingual masked language modelling to obtain the linguistic encoder. Moreover, the input resolution of visual encoder is 256×256 , and the input token length of the linguistic encoder is 256. The final image and text features are projected to the same dimension, which is 512 as [13], followed by batch normalization before interaction. The dimension of cross-lingual text alignment regularization (CTR) is set to 1024. More sensitivity analysis can be found in Sec E.5.

Image Data Pre-processing The original CXR images from the MIMIC-CXR and PadChest datasets [38, 39] are resized to 256×256 and randomly cropped to 224×224 , following the procedure in [5, 6, 7]. All images are normalized to the range $[0, 1]$. For data augmentation during pre-training, we apply horizontal flip, random rotation in the range $[0^\circ, 180^\circ]$, and auto contrast using the PyTorch vision library¹. The English and Spanish CXR image examples and its corresponding reports are depicted in Fig 6 and Fig 7, respectively.

Vision-language Pre-training Setup The detailed hyperparameters of vision-language pre-training for Med-UniC are shown in Tab 9. We use a cosine annealing scheduler for the adjustment of the learning rate. The pre-training step is conducted by V100 GPUs. To save GPU memory and speed up training, we also adopt automatic mixed-precision FP16.

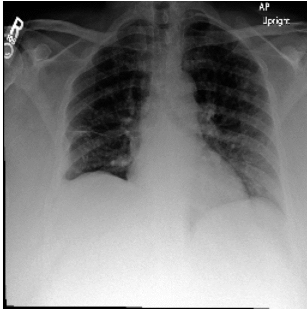
D Configurations for downstream Tasks

This section provides a detailed introduction to all downstream tasks and presents the data split information for each task. The data split details are presented in Tab 10.

Medical Image Linear Classification We explain the setting of linear classification tasks, including CheXpert [23], RSNA [43], and COVIDx [44]. We utilize ResNet-50, ViT-B/16 and ViT-L/32 as our visual backbone and fine-tune the linear layer with 50 epochs using early stop, with the same learning rate of 5e-4 and the default batch size is 8. We leverage the AdamW optimizer to schedule the learning rate, with the β_1 of 0.9, the β_2 of 0.999, and the weight decay rate of 1e-6. All the linear classification tasks are conducted on a V100 GPU with 32GB memory.

Medical Image Semantic Segmentation For the segmentation tasks RSNA and SIIM [46], we first adopt the ResNet-50 as the visual backbone and train the segmentation network on a 32G V100 GPU. We leverage early stopping to train the tasks for 50 and 100 epochs. We adapt 5e-4 as the learning rate, 1e-8 as the weight decay and 4 as the default batch size. We also employ AdamW as the optimizer and set the β_1 and β_2 as 0.9 and 0.999, respectively. For the ViT-B/16 and ViT-L/32 backbones, we set the training configurations following [59, 7].

¹<https://pytorch.org/vision/stable/transforms.htmls>



(a) CXR image example 1 from MIMIC dataset

Subject ID: 10000935

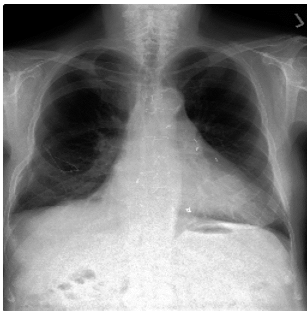
Study ID: 56164612

Report:

Lung volumes are low The heart size is normal.
The mediastinal and hilar contours are unremarkable.
New nodular opacities are clustered within the left upper lobe, and to a lesser extent, within the right upper lobe.

.....
Findings are compatible with metastases, as was noted in the lung bases on the subsequent CT of the abdomen and pelvis performed later the same day.

(b) CXR report example 1 from MIMIC dataset



(c) CXR image example 2 from MIMIC dataset

Subject ID: 10002430

Study ID: 58911492

Report:

The lung volumes are normal.
Mild cardiomegaly which is stable.
Normal hilar and mediastinal structures.

.....
Status post CABG with aligned median sternotomy wires and normal location of surgical clips.
Status post right lung surgery with surgical material seen.
Mild cardiomegaly No evidence of pneumonia

(d) CXR report example 2 from MIMIC dataset

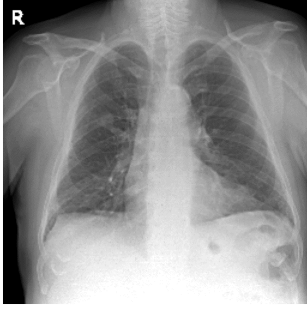
Figure 6: English CXR dataset examples.

Table 10: Data Split Details, ‘/’ indicates that no training/validation data is required in the zero-shot classification task.

Task	Dataset	Split	Train	Valid	Test
Linear Classification	CheXpert [23]	[23]	186,027	5,000	202
	RSNA [43]	[7, 43]	16,010	5,337	5,337
	COVIDx [44]	[7, 44]	23988	5998	400
Semantic Segmentation	RSNA [43]	[6, 7]	16,010	5,337	5,337
	SIIM [46]	[6, 7]	8,433	1,807	1,807
Object Detection	RSNA [43]	[6, 7]	16,010	5,337	5,337
	Object-CXR [48]	[7]	6,400	1,600	1,000
Zero-shot Classification	CXP500 [45]	[45]	/	/	500
	PDC [39]	[39]	/	/	1000

Medical Image Object Detection The Object Detection tasks RSNA and Object-CXR [48] are conducted on 1 V100 GPU. We use the grid search to find the optimal batch size as shown in Tab ?? . Specifically, we also adapt AdamW as our optimizer with the learning rate of $5e-4$, weight decay of $1e-6$, β_1 , β_2 of 0.9 and 0.999, batch size of 4. The IOU and NMS thresholds are [0.4, 0.45, 0.5, 0.55, 0.6, 0.65, 0.7, 0.75] and 0.5, respectively. We use ResNet-50 as the visual encoder of Med-UinC for fair comparisons with other baselines.

Zero-shot Task The original image undergoes a two-step process. Firstly, it is resized to dimensions of 256×256 and then center cropped to 224×224 . Subsequently, all pixel values are normalized within the range of $[0, 1]$, following [6, 7]. The resulting resized image is then passed through an image encoder to generate an image embedding . Concurrently, the prompts are inputted into a text encoder to obtain a text embeddings. To evaluate the classification, we measure the cosine similarity



(a) CXR image example 1 from PadChest dataset

Study ID: 216840111366964013217898866992011329134906098

Report:

Nodul proyect lsd 1 4 cm contorn parcial bien defin cit tac torac.
Patron intersticial con probabl are panalizacion bibasal probabl
fibrosis pulmon.

(b) CXR image example 1 from PadChest dataset



(c) CXR image example 2 from PadChest dataset

Study ID: 216840111366964013515091760022012318080539431

Report:

Fractur arcos costal lateral derech cuart quint sext septim.
Condensacion subsegmentari lii descart aspiracion sobreinfeccion
respiratori.
Pinzamient sen costofren izquierd.

(d) CXR image example 2 from PadChest dataset

Figure 7: Spanish CXR dataset examples.

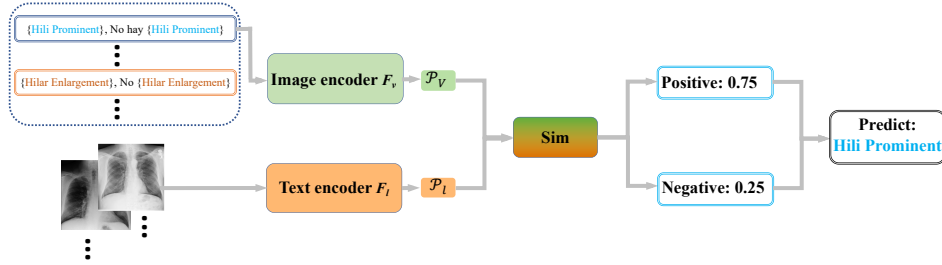


Figure 8: An example of Med-UniC zero-shot pipeline. Blue and orange denote Spanish and English prompts, respectively.

between the image and text embeddings for each prompt associated with a specific class. This is computed using the equation:

$$\text{sim}(\text{img}, \text{prompt}) = \mathcal{P}_v(\mathbf{v}_{e,i})^T \mathcal{P}_l(\mathbf{l}_{e,i}) \quad (8)$$

where $\mathbf{v}_{e,i}$ and $\mathbf{l}_{e,i}$ are image and text embeddings from visual and linguistic encoders, respectively. \mathcal{P}_v and \mathcal{P}_l are visual and linguistic projectors. The classification outcome is determined based on the comparison of cosine similarities. If the cosine similarity between the image embedding and the positive prompt (e.g., *disease*) exceeds the cosine similarity between the image embedding and the corresponding negative prompt (e.g., *No disease*), the outcome is considered positive. Conversely, if the reverse is true, the outcome is negative. The pipeline is detailed in Fig 8. To compute the performance metrics, the macro AUC score and F1 score, we calculate these scores for each category individually and then average them across all categories.

Table 11: Comparisons of different backbones on medical image segmentation tasks. Best results of each setting are in boldface.

Backbone	RSNA			SIIM		
	1%	10%	100%	1%	10%	100%
ResNet-50	72.6	74.4	76.7	56.7	62.2	64.4
ViT-B/16	75.6	76.6	77.9	62.1	67.3	71.5
ViT-L/32	74.4	77.5	78.7	64.5	68.7	73.3

E Additional Experimental Analysis

E.1 Tokenization Analysis of Cross-lingual Medical LM

Input Spanish report:

'infiltr alveor ambos camp pulmonar predomini derech bibasal sin grand cambi relacion rx previ 11 03 2017 .
derram pleural bilateral . catet venos con extrem proyect vcs .'

Tokens of CXR-BERT tokenizer:

['inf', '##itr', 'alve', '##or', 'amb', '##os', 'camp', 'pulmon', '##ar', 'predom', '##ini', 'dere', '##ch', 'bibas', '##al',
'sin', 'grand', 'camb', '##i', 'rel', '##aci', '##on', 'rx', 'prev', '##i', '11', '03', '2017', '.', 'der', '##ram', 'pleural',
'bilateral', '.', 'cat', '##et', 'veno', '##s', 'con', 'extrem', 'pro', '##ye', '##ct', 'vc', '##s', '.']

Tokens of Cross-lingual medical LM tokenizer:

['infiltr', 'alveor', 'amb', '##os', 'camp', 'pulmonar', 'predomini', 'derech', 'bibasal', 'sin', 'grand', 'cambi', 'relacion',
'rx', 'previ', '11', '03', '2017', '.', 'derram', 'pleural', 'bilateral', '.', 'catet', 'venos', 'con', 'extrem', 'proyect', 'vcs', '.']

Figure 9: Tokenization visualization of one Spanish report sample. Blue tokens represent tokenized words in the Spanish medical vocabulary of cross-lingual medical LM.

In this section, we visualize the tokenization results of one random selected Spanish report generated by CXR-BERT and Cross-lingual Medical LM’ tokenizers, respectively. As shown in Fig 9, compared with CXR-BERT, Cross-lingual Medical LM’s tokenizer can handle the Spanish sentence correctly and give a tokenized scheme without loss of Spanish words’ semantics. However, CXR-BERT’s tokenizer uses tokens from its English medical vocabulary may deteriorate the original Spanish semantics. The visualization results demonstrate the importance of building a cross-lingual lexicon from Spanish medical reports.

E.2 Medical Image Segmentation with ViT Backbone

In this section, we adopt the ViT-B/16 and ViT-L/32 as the visual encoder of Med-UniC to compare with ResNet-50 for medical image segmentation tasks on RSNA and SIIM datasets. As shown in Tab 11, surprisingly, the ViT-B/16 backbone has noticeable improvement compared with the ResNet-50 backbone, especially for SIIM. Additionally, the ViT-L/32 backbone shows better results than ViT-B/16 in most settings, indicating that larger visual backbone can further improve the performance of Med-UniC. We attribute this enhancement from the ViT backbone to the global attention capability of the transformer-based visual encoder on segmentation [59].

Table 12: Ablation Study on CTR. Best results of each setting are in boldface, and the '-' denotes mAP values smaller than 1%.

Backbone	COVIDx(ACC)			RSNA(Dice)			Object CXR(mAP)		
	1%	10%	100%	1%	10%	100%	1%	10%	100%
\mathcal{L}_{CTR}	76.5	89.0	92.8	72.6	74.4	76.7	6.6	13.3	21.6
\mathcal{L}_{CTR} (w/o \mathcal{L}_{TF})	74.9	86.2	92.3	72.2	72.9	74.4	-	12.3	19.9
\mathcal{L}_{CTR} (w/o \mathcal{L}_{TT})	75.8	87.4	92.5	71.6	73.5	75.6	4.5	12.9	20.5

Table 13: Ablation Study on VLP data, The best results for each setting are highlighted in bold, and the ‘-’ denotes mAP values smaller than 1%. Methods with * leverage disease-level annotations. † denotes that Med-UniC only pre-trained on MIMIC dataset (En). Best results of each setting are in boldface.

Backbone	COVIDx(ACC)			RSNA(Dice)			Object CXR(mAP)		
	1%	10%	100%	1%	10%	100%	1%	10%	100%
ConVIRT[5]	67.3	77.8	89.0	55.0	67.4	67.5	-	8.6	15.9
GLoRIA-MIMIC[6]	66.5	80.5	88.8	60.3	68.7	68.3	-	8.9	16.6
MGCA* [7]	74.5	85.2	90.3	63.0	68.3	69.8	-	12.1	19.2
MedKLIP* [8]	72.0	83.5	90.5	66.2	69.4	71.9	-	7.1	11.6
Med-UniC (En) [†]	74.7	85.5	91.3	70.4	71.2	73.5	3.4	12.5	19.5
Med-UniC	76.5	89.0	92.8	72.6	74.4	76.7	6.6	13.3	21.6

E.3 Ablation Study on Cross-lingual Text Alignment Regularization

In this part, we explore the influence of each sub-component belonging to Cross-lingual Text Alignment Regularization \mathcal{L}_{CTR} , including text-feature alignment \mathcal{L}_{TF} and text-to-text alignment \mathcal{L}_{TT} . As shown in Tab 12, reducing \mathcal{L}_{TT} or \mathcal{L}_{TF} can both lead to performance drop. Specifically, removing \mathcal{L}_{TF} shows worse results than removing \mathcal{L}_{TT} on most of settings, demonstrating the importance of learning cross-lingual invariance and reducing the languages bias through \mathcal{L}_{TF} .

E.4 Med-UniC Pre-training on Uni-lingual data

On the basis of Med-UniC paradigm, we further study the performance of only using the uni-lingual MIMIC dataset for pre-training. The ablation results are shown in Tab 13, which reveals that although using uni-lingual data to pre-train Med-UniC causes performance drop, compared to other baselines, our framework can also bring benefits. We attribute this to the self-supervised vision alignment (SSV) to learn more exhaustive visual representation and text-to-text alignment to keep in-modal consistency.

Table 14: Dimension Analysis of Projector \mathcal{P}_d . Best results of each setting are in boldface.

Dimension	COVIDx(ACC)			RSNA(Dice)			Object CXR(mAP)		
	1%	10%	100%	1%	10%	100%	1%	10%	100%
512	75.5	87.9	92.2	72.4	73.8	74.5	3.8	12.9	20.8
1024	76.5	89.0	92.8	72.6	74.4	76.7	6.6	13.3	21.6
2048	75.9	88.7	92.5	73.1	74.2	76.5	4.6	13.1	22.5

E.5 Embedding Dimension Analysis of Text Alignment Projector \mathcal{P}_d

In this section, we investigate the impact of output dimension D' from text alignment projector \mathcal{P}_d , since D' determines the size of cross-correlation matrix $\tilde{\mathbf{Z}}_e$ for text-feature alignment. We experiment with linear classification, segmentation and object detection, respectively. Tab 14 shows the corresponding results with different dimensions. When the dimension size is 1024, it can achieve better results on most of the experimental settings. Hence, we take $D' = 1024$ as our default setting during the pre-training.

References

- [1] M. Ni, H. Huang, L. Su, E. Cui, T. Bharti, L. Wang, D. Zhang, and N. Duan, “M3p: Learning universal representations via multitask multilingual multimodal pre-training,” in *Proceedings of the IEEE/CVF conference on computer vision and pattern recognition*, 2021, pp. 3977–3986.

- [2] M. Zhou, L. Zhou, S. Wang, Y. Cheng, L. Li, Z. Yu, and J. Liu, "Uc2: Universal cross-lingual cross-modal vision-and-language pre-training," in *Proceedings of the IEEE/CVF Conference on Computer Vision and Pattern Recognition*, 2021, pp. 4155–4165.
- [3] A. Jain, M. Guo, K. Srinivasan, T. Chen, S. Kudugunta, C. Jia, Y. Yang, and J. Baldridge, "MURAL: Multimodal, multitask representations across languages," in *Findings of the Association for Computational Linguistics: EMNLP 2021*, Nov. 2021.
- [4] Y. Zeng, W. Zhou, A. Luo, and X. Zhang, "Cross-view language modeling: Towards unified cross-lingual cross-modal pre-training," *arXiv preprint arXiv:2206.00621*, 2022.
- [5] Y. Zhang, H. Jiang, Y. Miura, C. D. Manning, and C. P. Langlotz, "Contrastive learning of medical visual representations from paired images and text," *arXiv preprint arXiv:2010.00747*, 2020.
- [6] S.-C. Huang, L. Shen, M. P. Lungren, and S. Yeung, "Gloria: A multimodal global-local representation learning framework for label-efficient medical image recognition," in *Proceedings of the IEEE/CVF International Conference on Computer Vision*, 2021, pp. 3942–3951.
- [7] F. Wang, Y. Zhou, S. Wang, V. Vardhanabhuti, and L. Yu, "Multi-granularity cross-modal alignment for generalized medical visual representation learning," *arXiv preprint arXiv:2210.06044*, 2022.
- [8] C. Wu, X. Zhang, Y. Zhang, Y. Wang, and W. Xie, "Medklip: Medical knowledge enhanced language-image pre-training," *medRxiv*, pp. 2023–01, 2023.
- [9] H.-Y. Zhou, C. Lian, L. Wang, and Y. Yu, "Advancing radiograph representation learning with masked record modeling," in *The Eleventh International Conference on Learning Representations*.
- [10] S. Long, F. Cao, S. C. Han, and H. Yang, "Vision-and-language pretrained models: A survey."
- [11] OpenAI, "Gpt-4 technical report," *ArXiv*, vol. abs/2303.08774, 2023.
- [12] A. Kirillov, E. Mintun, N. Ravi, H. Mao, C. Rolland, L. Gustafson, T. Xiao, S. Whitehead, A. C. Berg, W.-Y. Lo *et al.*, "Segment anything," *arXiv preprint arXiv:2304.02643*, 2023.
- [13] M. Oquab, T. Darcet, T. Moutakanni, H. Vo, M. Szafraniec, V. Khalidov, P. Fernandez, D. Haziza, F. Massa, A. El-Nouby *et al.*, "Dinov2: Learning robust visual features without supervision," *arXiv preprint arXiv:2304.07193*, 2023.
- [14] A. Gilson, C. Safranek, T. Huang, V. Socrates, L. Chi, R. A. Taylor, and D. Chartash, "How well does chatgpt do when taking the medical licensing exams? the implications of large language models for medical education and knowledge assessment," *medRxiv*, pp. 2022–12, 2022.
- [15] T. H. Kung, M. Cheatham, A. Medenilla, C. Sillos, L. De Leon, C. Elepaño, M. Madriaga, R. Aggabao, G. Diaz-Candido, J. Maningo *et al.*, "Performance of chatgpt on usml: Potential for ai-assisted medical education using large language models," *PLoS digital health*, vol. 2, no. 2, p. e0000198, 2023.
- [16] Y. Huang, X. Yang, L. Liu, H. Zhou, A. Chang, X. Zhou, R. Chen, J. Yu, J. Chen, C. Chen *et al.*, "Segment anything model for medical images?" *arXiv preprint arXiv:2304.14660*, 2023.
- [17] W. Ji, J. Li, Q. Bi, W. Li, and L. Cheng, "Segment anything is not always perfect: An investigation of sam on different real-world applications," *arXiv preprint arXiv:2304.05750*, 2023.
- [18] S. He, R. Bao, J. Li, P. E. Grant, and Y. Ou, "Accuracy of segment-anything model (sam) in medical image segmentation tasks," *arXiv preprint arXiv:2304.09324*, 2023.
- [19] N. Mu, A. Kirillov, D. Wagner, and S. Xie, "Slip: Self-supervision meets language-image pre-training," in *European Conference on Computer Vision*. Springer, 2022, pp. 529–544.
- [20] B. Boecking, N. Usuyama, S. Bannur, D. C. de Castro, A. Schwaighofer, S. L. Hyland, M. T. A. Wetscherek, T. Naumann, A. Nori, J. Alvarez-Valle, H. Poon, and O. Oktay, "Making the most of text semantics to improve biomedical vision-language processing," *ArXiv, ECCV*.
- [21] A. Bustos, A. Pertusa, J. M. Salinas, and M. de la Iglesia-Vayá, "Padchest: A large chest x-ray image dataset with multi-label annotated reports," *Medical image analysis*, vol. 66, p. 101797, 2019.
- [22] A. E. W. Johnson, T. J. Pollard, S. J. Berkowitz, N. R. Greenbaum, M. P. Lungren, C. ying Deng, R. G. Mark, and S. Horng, "Mimic-cxr, a de-identified publicly available database of chest radiographs with free-text reports," *Scientific Data*, vol. 6, 2019.
- [23] J. Irvin, P. Rajpurkar, M. Ko, Y. Yu, S. Ciurea-Ilicus, C. Chute, H. Marklund, B. Haghgoo, R. Ball, K. Shpanskaya *et al.*, "Chexpert: A large chest radiograph dataset with uncertainty labels and expert comparison," in *Proceedings of the AAAI conference on artificial intelligence*, vol. 33, 2019, pp. 590–597.
- [24] J. Devlin, M.-W. Chang, K. Lee, and K. Toutanova, "Bert: Pre-training of deep bidirectional transformers for language understanding," *ArXiv*, vol. abs/1810.04805, 2019.
- [25] ———, "Bert: Pre-training of deep bidirectional transformers for language understanding," *arXiv preprint arXiv:1810.04805*, 2018.

- [26] I. J. Goodfellow, M. Mirza, X. Da, A. C. Courville, and Y. Bengio, “An empirical investigation of catastrophic forgetting in gradient-based neural networks,” *CoRR*, vol. abs/1312.6211, 2013.
- [27] A. Radford, J. W. Kim, C. Hallacy, A. Ramesh, G. Goh, S. Agarwal, G. Sastry, A. Askell, P. Mishkin, J. Clark *et al.*, “Learning transferable visual models from natural language supervision,” in *International Conference on Machine Learning*. PMLR, 2021, pp. 8748–8763.
- [28] A. van den Oord, Y. Li, and O. Vinyals, “Representation learning with contrastive predictive coding,” *ArXiv*, vol. abs/1807.03748, 2018.
- [29] J. Singh, B. McCann, R. Socher, and C. Xiong, “Bert is not an interlingua and the bias of tokenization,” in *Conference on Empirical Methods in Natural Language Processing*, 2019.
- [30] R. Xian, H. Ji, and H. Zhao, “Cross-lingual transfer with class-weighted language-invariant representations,” in *International Conference on Learning Representations*, 2022.
- [31] A. Lauscher, V. Ravishankar, I. Vulic, and G. Glavas, “From zero to hero: On the limitations of zero-shot language transfer with multilingual transformers,” in *Conference on Empirical Methods in Natural Language Processing*, 2020.
- [32] K. K. Z. Wang, S. Mayhew, and D. Roth, “Cross-lingual ability of multilingual bert: An empirical study,” *International Conference on Learning Representations*, vol. abs/1912.07840, 2020.
- [33] P. Dufter and H. Schütze, “Identifying elements essential for bert’s multilinguality,” in *Conference on Empirical Methods in Natural Language Processing*, 2020.
- [34] J. Zhang and Z. Lan, “S-simcse: Sampled sub-networks for contrastive learning of sentence embedding,” *Conference on Empirical Methods in Natural Language*, 2021.
- [35] H. B. Barlow, “Redundancy reduction revisited,” *Network: Computation in Neural Systems*, vol. 12, pp. 241 – 253, 2001.
- [36] J. Zbontar, L. Jing, I. Misra, Y. LeCun, and S. Deny, “Barlow twins: Self-supervised learning via redundancy reduction,” in *International Conference on Machine Learning*, 2021.
- [37] S. Goel, H. Bansal, S. K. Bhatia, R. A. Rossi, V. Vinay, and A. Grover, “Cyclip: Cyclic contrastive language-image pretraining,” *NIPS*, 2022.
- [38] A. E. Johnson, T. J. Pollard, N. R. Greenbaum, M. P. Lungren, C.-y. Deng, Y. Peng, Z. Lu, R. G. Mark, S. J. Berkowitz, and S. Horng, “Mimic-cxr-jpg, a large publicly available database of labeled chest radiographs,” *arXiv preprint arXiv:1901.07042*, 2019.
- [39] A. Bustos, A. Pertusa, J.-M. Salinas, and M. de la Iglesia-Vayá, “Padchest: A large chest x-ray image dataset with multi-label annotated reports,” *Medical image analysis*, vol. 66, p. 101797, 2020.
- [40] K. He, X. Zhang, S. Ren, and J. Sun, “Deep residual learning for image recognition,” in *Proceedings of the IEEE conference on computer vision and pattern recognition*, 2016, pp. 770–778.
- [41] A. Dosovitskiy, L. Beyer, A. Kolesnikov, D. Weissenborn, X. Zhai, T. Unterthiner, M. Dehghani, M. Minderer, G. Heigold, S. Gelly *et al.*, “An image is worth 16x16 words: Transformers for image recognition at scale,” *arXiv preprint arXiv:2010.11929*, 2020.
- [42] I. Loshchilov and F. Hutter, “Decoupled weight decay regularization,” *arXiv preprint arXiv:1711.05101*, 2017.
- [43] G. Shih, C. C. Wu, S. S. Halabi, M. D. Kohli, L. M. Prevedello, T. S. Cook, A. Sharma, J. K. Amorosa, V. Arteaga, M. Galperin-Aizenberg *et al.*, “Augmenting the national institutes of health chest radiograph dataset with expert annotations of possible pneumonia,” *Radiology: Artificial Intelligence*, vol. 1, no. 1, p. e180041, 2019.
- [44] L. Wang, Z. Q. Lin, and A. Wong, “Covid-net: A tailored deep convolutional neural network design for detection of covid-19 cases from chest x-ray images,” *Scientific reports*, vol. 10, no. 1, pp. 1–12, 2020.
- [45] A. Saporta, X. Gui, A. Agrawal, A. Pareek, S. Q. Truong, C. D. Nguyen, V.-D. Ngo, J. Seekins, F. G. Blankenberg, A. Y. Ng *et al.*, “Benchmarking saliency methods for chest x-ray interpretation,” *Nature Machine Intelligence*, vol. 4, no. 10, pp. 867–878, 2022.
- [46] C. Steven G. Langer, PhD and M. George Shih, MD, “Siim-acr pneumothorax segmentation,” 2019.
- [47] O. Ronneberger, P. Fischer, and T. Brox, “U-net: Convolutional networks for biomedical image segmentation,” in *Medical Image Computing and Computer-Assisted Intervention–MICCAI 2015: 18th International Conference, Munich, Germany, October 5–9, 2015, Proceedings, Part III 18*. Springer, 2015, pp. 234–241.
- [48] J. Healthcare, “Object-cxr-automatic detection of foreign objects on chest x-rays,” 2020.
- [49] J. Redmon and A. Farhadi, “Yolov3: An incremental improvement,” *arXiv preprint arXiv:1804.02767*, 2018.

- [50] K. He, X. Chen, S. Xie, Y. Li, P. Doll’ar, and R. B. Girshick, “Masked autoencoders are scalable vision learners,” *2022 IEEE/CVF Conference on Computer Vision and Pattern Recognition (CVPR)*, pp. 15 979–15 988, 2021.
- [51] R. R. Selvaraju, A. Das, R. Vedantam, M. Cogswell, D. Parikh, and D. Batra, “Grad-cam: Visual explanations from deep networks via gradient-based localization,” *International Journal of Computer Vision*, vol. 128, pp. 336–359, 2016.
- [52] M. Oquab, T. Darcet, T. Moutakanni, H. Q. Vo, M. Szafraniec, V. Khalidov, P. Fernandez, D. Haziza, F. Massa, A. El-Nouby, M. Assran, N. Ballas, W. Galuba, R. Howes, P.-Y. Huang, S.-W. Li, I. Misra, M. G. Rabbat, V. Sharma, G. Synnaeve, H. Xu, H. Jégou, J. Mairal, P. Labatut, A. Joulin, and P. Bojanowski, “Dinov2: Learning robust visual features without supervision,” *ArXiv*, vol. abs/2304.07193, 2023.
- [53] Z. Wan, Y. Yin, W. Zhang, J. Shi, L. Shang, G. Chen, X. Jiang, and Q. Liu, “G-map: General memory-augmented pre-trained language model for domain tasks,” in *Conference on Empirical Methods in Natural Language Processing*, 2022.
- [54] J. Li, C. Liu, S. Cheng, R. Arcucci, and S. Hong, “Frozen language model helps ecg zero-shot learning,” in *Medical Imaging with Deep Learning*, 2023.
- [55] S. Cheng, C. Quilodrán-Casas, S. Ouala, A. Farchi, C. Liu, P. Tando, R. Fablet, D. Lucor, B. Iooss, J. Brajard *et al.*, “Machine learning with data assimilation and uncertainty quantification for dynamical systems: a review,” *arXiv preprint arXiv:2303.10462*, 2023.
- [56] S. Cheng, I. C. Prentice, Y. Huang, Y. Jin, Y.-K. Guo, and R. Arcucci, “Data-driven surrogate model with latent data assimilation: Application to wildfire forecasting,” *Journal of Computational Physics*, vol. 464, p. 111302, 2022.
- [57] C. Liu, R. Fu, D. Xiao, R. Stefanescu, P. Sharma, C. Zhu, S. Sun, and C. Wang, “Enkf data-driven reduced order assimilation system,” *Engineering Analysis with Boundary Elements*, vol. 139, pp. 46–55, 2022.
- [58] Z. Wan, B. Wang, X. Liu, J. Qiu, B. Li, T. Guo, G. Chen, and Y. Wang, “Spatio-temporal contrastive learning enhanced gns for session-based recommendation,” *ArXiv*, vol. abs/2209.11461, 2022.
- [59] S. Zheng, J. Lu, H. Zhao, X. Zhu, Z. Luo, Y. Wang, Y. Fu, J. Feng, T. Xiang, P. H. S. Torr, and L. Zhang, “Rethinking semantic segmentation from a sequence-to-sequence perspective with transformers,” *2021 IEEE/CVF Conference on Computer Vision and Pattern Recognition (CVPR)*, pp. 6877–6886, 2020.